Hierarchical Multimodel Saltwater Intrusion Remediation and Sampling Designs: A BMA Tree Approach

Basic Information

Title:	Hierarchical Multimodel Saltwater Intrusion Remediation and Sampling Designs: A BMA Tree Approach
Project Number:	2010LA76G
Start Date:	9/1/2010
End Date:	8/31/2013
Funding Source:	104G
Congressional District:	Louisiana
Research Category:	Ground-water Flow and Transport
Focus Category:	Groundwater, Management and Planning, Methods
Descriptors:	None
Principal Investigators:	Frank Tsai, Jeff Hanor

Publications

1. Tsai, F.T.-C. (2011). Scavenger Wells Stop Saltwater Intrusion in Baton Rouge, Louisiana, IGWMC MODFLOW and More 2011 Conference: Integrated Hydrologic Modeling, Golden, Colorado, June 5-8, 2011.
2. Tsai, F. T.-C., and Ahmed S. Elshall (2011). A Hierarchical Bayesian Model Averaging Approach to Cope With Sources of Uncertainty in Conceptual Ground Water Models, World Water & Environmental Resources Congress, Palm Springs, California, May 22-26, 2011.
3. Tsai, F. T.-C. (2011). Stop Saltwater Intrusion Toward Water Wells Using Scavenger Wells, World Water & Environmental Resources Congress, Palm Springs, California, May 22-26, 2011.
4. Callie E. Anderson and Jeffrey S. Hanor (2011) Origin of waters causing salinization of the Baton Rouge aquifer system, Louisiana. South-Central Section Geological Society of America 45th Annual Meeting, March 27-29, 2011.
5. Frank T.-C. Tsai (2011). Saltwater Intrusion Simulation in the “1,500-Foot” Sand of the Baton Rouge Area: Pre-Anthropogenic Pumping, Current Situation, Future, Fifth Annual Louisiana Groundwater, Coastal Geology and Subsidence-Land Loss Symposia, Baton Rouge, Louisiana, January 11-12, 2011.
6. Callie E. Anderson and Jeffrey S. Hanor (2011) The St. Gabriel salt dome as a potential source of the salty waters contaminating the Baton Rouge aquifer system. Fifth Annual Louisiana Groundwater, Coastal Geology and Subsidence-Land Loss Symposia, Baton Rouge, Louisiana, January 11-12, 2011.
7. Ahmed Elshall and Frank T.-C. Tsai (2011). Geophysical and geostatistical approaches to subsurface characterization of the Baton Rouge area, Fifth Annual Louisiana Groundwater, Coastal Geology and Subsidence-Land Loss Symposia, Baton Rouge, Louisiana, January 11-12, 2011.
8. Nima Chitsazan and Frank T.-C. Tsai (2011). Bed boundary delineation of “1,500-foot’, “1,700-foot”, and “2,000-foot sands of the Baton Rouge area, Fifth Annual Louisiana Groundwater, Coastal Geology and Subsidence-Land Loss Symposia, Baton Rouge, Louisiana, January 11-12, 2011.
9. Tsai, F. T.-C. (2010). “1,500-Foot” Sand Saltwater Intrusion Simulation and Management Using Scavenger Wells, Baton Rouge Geological Society, Baton Rouge, Louisiana, December 10, 2010. (invited)

10. Tsai, F.T.-C. (2010), Scavenger Wells Stop Saltwater Intrusion in Baton Rouge, 2010 Louisianan Water Quality Technology Conference, Alexandria and Baton Rouge, Louisiana, December 14-15, 2010. (invited)
11. Tsai, F.T.-C. (2010) Scavenger Well Operation to Stop Saltwater Intrusion Toward BRWC Lula Wells in the Baton Rouge Area, Louisiana Capital Area Ground Water Conservation Commission, September 14, 2010. (invited)
12. • Frank Tsai, 2012, Feasibility Study of Scavenging Approach to Stop Saltwater Toward Water Wells, Louisiana State University, Baton Rouge, Louisiana, 10 pages. (USGS 104B)
13. Tsai, F. T.-C., and A.S. Elshall. (2011). A Hierarchical Bayesian Model Averaging Approach to Cope With Sources of Uncertainty in Conceptual Ground Water Models, World Water & Environmental Resources Congress, Palm Springs, CA, May 22-26, 2011.
14. Tsai, F. T.-C. (2011). Development of Scavenger Well Operation Model To Stop Saltwater Intrusion Toward Water Wells In The "1,500-Foot" Sand of The Baton Rouge Area, Louisiana, World Water & Environmental Resources Congress, Palm Springs, CA, May 22-26, 2011.
15. Tsai, F. T.-C. (2011). Scavenger Wells Stop Saltwater Intrusion in Baton Rouge, Louisiana, MODFLOW and More 2011, Golden, CO, June 5-8, 2011

SYNOPSIS

Title: Hierarchical Multimodel Saltwater Intrusion Remediation and Sampling Designs: A BMA Tree Approach
Project Number: G10AP00136
Start Date: 9/1/2010
End Date: 8/31/2013
Funding Source: 104G
Research Category: Ground-water Flow and Transport
Focus Categories: GW, M&P, MET
Descriptors: Remediation Design, Sampling Design, Saltwater Intrusion, Optimization, Uncertainty
Primary PI: Frank T.-C. Tsai
Other PI: Jeffrey S. Hanor

Problem and Research Objectives

Water use in Baton Rouge, Louisiana is approximately 629,000 m^3 per day (166 million gallons per day) out of which 88% is ground water and the rest is surface water (Sargent, 2007). Due to excessive ground water pumping, saltwater is intruding from the saline aquifers in the south part of the Baton Rouge Fault. Thus, in the absence of any remediation measure, some of public supply water wells in East Baton Rouge Parish are under the threat of being abandoned in the near future. The project objective is to develop saltwater intrusion models to be employed for the management and remediation of the ground water resources for the study area shown in Figure 1. The study area is approximately 500 km^2. To ensure a valid saltwater intrusion model, the interim report develops stratigraphy models that capture the complexity and heterogeneity of the subsurface geology in the Baton Rouge area.

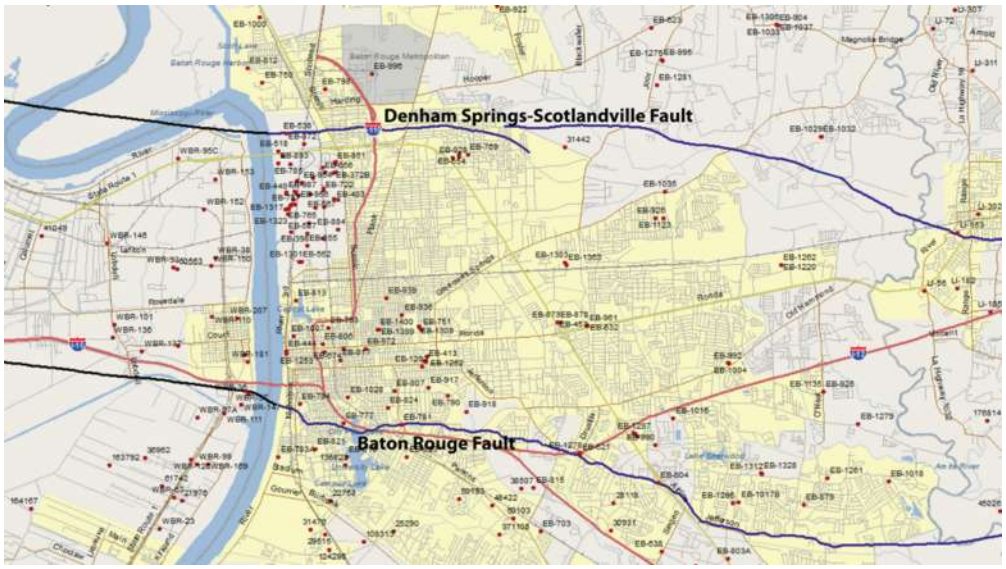

Figure 1: The study area. Red dots are electrical logs. The base map is created by Louisiana GIS Digital Map 2007. The fault lines are obtained from McCulloh and Heinrich (2012).

Due to limited amount of data and since model uncertainty always exists, multiple models are usually developed. Model selection, model elimination, model reduction, and model discrimination are commonly used to select the best model. It is clear that modeling uncertainty is always underestimated if only the best model is used. One would ask why only the best model is used afterwards when so many efforts have been devoted to calibrating many models. This certainly wastes valuable resources and important information from other good models. Hierarchical Bayesian model averaging (HBMA) best utilize all possible models for model prediction and application under Bayesian statistical framework. HBMA presents several advantages over model selection: (1) Information from all possible models is used based on their model importance (model weights). Calibration efforts are not wasted. (2) The model importance is based on the evidence of data, which avoids over-confidence in the best model that does not have a dominant model weight. And (3) model structure uncertainty is increased and is better presented than that by using a single model. Moreover, HBMA is able to distinguish model uncertainty arising from individual models and between models. HBMA is able to identify unfavorable models even though they may present small prediction uncertainty.

In this study, HBMA is used to construct stratigraphy for the Baton Rouge aquifer system. Indicator geostatistical techniques are used to analyze electrical resistivity logs and reconstruct the subsurface accordingly. The HBMA is applied to analyze the conceptual model structure uncertainty arising from the different sand-clay line cutoff values for the resistivity logs and the different sand-clay cutoff probabilities for the interpolated values.

Methodology

(1) Indicator Kriging

Given the volumetric domain $D \subset \mathbb{R}^n$, the indicator function $\{I(\boldsymbol{x}, v) : \boldsymbol{x} \in D\}$ is a random function. The indicator random variable v describes the spatial extension of a categorical variable C, which is the sand-clay distribution in aquifers under different sand-clay line cutoff $\propto$ as determined from the electrical resistivity logs. The random function of the indicator random variable of class C is defined as:

$$I(\boldsymbol{x}, v) = \begin{cases} 1 & v \in C,\ v(\boldsymbol{x}) > \propto \\ 0 & v \notin C,\quad v(\boldsymbol{x}) < \propto \end{cases} \tag{1}$$

where I=1 is sand and I=0 is clay in this study. The indicator function $I(\boldsymbol{x}, v)$ is a random function of two variables in which v is an outcome of random variable at location $\boldsymbol{x}$ in which the one and zero indicates the presence of sand and clay, respectively. The indicator variogram has the same definition as the normal variogram except that the real random function is replaced by the indicator random function $I(x)$ as follows

$$\gamma_I(h) = \frac{1}{2N(h)} \sum_{i=1}^{N(h)} [I(x_i - I(x_i + h)]^2 \tag{2}$$

where $N(h)$ is the number of pairs within the lag interval h. The main source of the sample data, which are used to generate the IK variograms, is from the electrical resistivity logs that are provided by the Louisianan Department of Natural Resources (DNR), the Department of Transportation and Development (DOTD), the United States Geological Survey (USGS), the Louisiana Geological Survey (LGS), and the Baton Rouge Water Company (BRWC). In the study area shown in Figure 1, we have more than 350 electrical logs.

For each foot and for every resistivity log location, the resistivity values indicate either sand or clay depending on the sand-clay line cutoff as determined from the clay line in the resistivity

curves. Another source of data is from the study of Wendeborn and Hanor (2008), in which they analyzed spontaneous potential (SP) curves to identify the sand-clay distribution along the Baton Rouge fault. The interpretation of these logs in terms of sand-clay sequences are amended to the main data to provide more sampling locations. All observation points are amended together through linear interpolation over each foot. The number of samples in each observation point varies from 800 to 3000 depending on the depth of each borehole. Thus, over a depth z with an increment of 1 foot, an experimental variogram is generated. A pseudo 3D horizontal experimental variogram is obtained by averaging all the 2D experimental variograms for all depths.

Under the basic assumption that the sample domain is stationary, ergodic and sufficient to reliable reproduce the statistics, the obtained theoretical variogram is used for the indicator kriging interpolation as a method for constructing the subsurface stratigraphy. The aim of kriging is to estimate the value of a random variable at unsampled points. Over a defined cell size, which is $200\,m \times 200\,m$ in this study, indicator kriging uses weighted average of the neighboring sample data points to estimate the indicator value in each cell using the following system of equations:

$$\begin{bmatrix} \gamma(x_1,x_1) & \gamma(x_1,x_2) & \mathrm{L} & \gamma(x_1,x_N) & 1 \\ \gamma(x_2,x_1) & \gamma(x_2,x_2) & \mathrm{L} & \gamma(x_2,x_N) & 1 \\ \mathrm{M} & \mathrm{M} & \mathrm{L} & \mathrm{M} & \mathrm{M} \\ \gamma(x_N,x_1) & \gamma(x_N,x_2) & \mathrm{L} & \gamma(x_N,x_N) & 1 \\ 1 & 1 & \mathrm{L} & 1 & 0 \end{bmatrix} \begin{bmatrix} \lambda_1 \\ \lambda_2 \\ \mathrm{M} \\ \lambda_N \\ L \end{bmatrix} = \begin{bmatrix} \gamma(x_1,x_0) \\ \gamma(x_2,x_0) \\ \mathrm{M} \\ \gamma(x_N,x_0) \\ 1 \end{bmatrix} \text{ or } A\lambda = b \tag{3}$$

in which $\gamma(x_i, x_j)$ is the variogram of v between the data points x_i and x_j , and the $\gamma(x_i, x_o)$ is the variogram between the data point x_i and the target point x_o. To guarantee that the estimates are unbiased, the sum of the weights λ_i is one. The unbiased constrained is imbedded to the minimization problem through the use of the Lagrange multiplier L. Once the weights for each data point are obtained, the last step is to calculate the expected indicator value and the indicator kriging variance by using the following equations.

$$v^*(x_0) = \sum_{i=1}^{N} \lambda_i I(x_i) \quad and \quad \sigma_{IK}^2 = b^T \lambda \tag{4}$$

(2) Hierarchical Bayesian Model Averaging (HBMA)

To cope with sources of uncertainty in stratigraphy models, a hierarchical Bayesian model averaging is developed. Consider $\mathrm{M}_{\underbrace{(\mathrm{ij}\ldots\mathrm{lm})}_{\mathrm{p}}} \in \mathbf{M}_\mathrm{p}$ a model at level p. The subscript $\underbrace{(\mathrm{ij}\ldots\mathrm{lm})}_{\mathrm{p}}$ locates the model hierarchically top down from the first level, to the second level and so forth to reach to level p. For example, $\mathrm{M}_{(\mathrm{i})} \in \mathbf{M}_1$ is model i at level 1, $\mathrm{M}_{(\mathrm{ij})} \in \mathbf{M}_2$ is model j at level 2, which is a child model to parent model i at level 1. $\mathrm{M}_{(\mathrm{ijk})} \in \mathbf{M}_3$ is model k at level 3, which is a child model to the parent model j at level 2 and the grandparent model of model i at level 1. From bottom up, parent models $\mathbf{M}_{\mathrm{p}-1}$ at level $\mathrm{p}-1$ is composed of the child models $\mathbf{M}_\mathrm{p}$ at level p. Models $\mathbf{M}_{\mathrm{p}-2}$ at level $\mathrm{p}-2$ are composed of models $\mathbf{M}_{\mathrm{p}-1}$ at level $\mathrm{p}-1$ and so forth until the Hierarch BMA model M_0 is reached.

Consider base models at level p. According to the law of total probability, the posterior probability for predicted quantity Δ given data $\mathbf{D}$ is

$$\Pr(\Delta \mid \mathbf{D}) = E_{M_1} E_{M_2} \mathrm{L}\ E_{M_p}\left[\Pr(\Delta \mid \mathbf{D}, \mathbf{M}_p)\right] \tag{5}$$

where E_{M_p} is the expectation operator with respect to models $\mathbf{M}_p$ at level p. $\Pr(\Delta|\mathbf{D}, \mathbf{M}_p)$ is the posterior probability of predicted quantity Δ given data $\mathbf{D}$ and models $\mathbf{M}_p$ at level p. The expectation $E_{M_p}[\Pr(\Delta|\mathbf{D}, \mathbf{M}_p)]$ is posterior probability averaging at level p. That is

$$E_{M_p}\left[\Pr(\Delta \mid \mathbf{D}, \mathbf{M}_p)\right] = \sum_m \Pr\left(\Delta \mid \mathbf{D}, M_{\underbrace{(ijL,lm)}_{p}}\right) \Pr\left(M_{\underbrace{(ijL,lm)}_{p}} \mid \mathbf{D}, M_{\underbrace{(ijL,l)}_{p-1}}\right). \tag{6}$$

where $\Pr\left(\Delta \mid \mathbf{D}, M_{\underbrace{(ijL,lm)}_{p}}\right) = \Pr(\Delta \mid \mathbf{D}, \mathbf{M}_p)$.

$\Pr\left(M_{\underbrace{(ijL,lm)}_{p}} \mid \mathbf{D}, M_{\underbrace{(ijL,l)}_{p-1}}\right) = \Pr(\mathbf{M}_p \mid \mathbf{D}, \mathbf{M}_{p-1})$ is the conditional posterior model probability of model $M_{\underbrace{(ij\ldots lm)}_{p}}$ at level p under model $M_{\underbrace{(ij\ldots l)}_{p-1}}$ at level $p-1$. $\Pr(\mathbf{M}_p \mid \mathbf{D}, \mathbf{M}_{p-1})$ also represents the conditional model weights and will be used to develop a BMA tree of model weights. Note that model $M_{(ij\ldots lm)}$ is a child model under the parent model $M_{(ij\ldots l)}$ because both have the same subscript for the first $p-1$ levels. Equation (6) is the Bayesian model averaging (BMA) at level p, which can be written as

$$\Pr(\Delta \mid \mathbf{D}, \mathbf{M}_{p-1}) = E_{M_p}\left[\Pr(\Delta \mid \mathbf{D}, \mathbf{M}_p)\right] \tag{7}$$

According to equations (5) and (7), one can derive the posterior probability of prediction using BMA over models at any level, say level n:

$$\Pr(\Delta \mid \mathbf{D}, \mathbf{M}_n) = E_{M_{n+1}} E_{M_{n+2}} \mathrm{L}\ E_{M_p}\left[\Pr(\Delta \mid \mathbf{D}, \mathbf{M}_p)\right]. \tag{8}$$

Based on equation (8), the law of total expectation and the law of total variance, the prediction mean, within-model variance, between model variance and total variance can be derived at level n.

In this study, Δ is the indicator value and $\mathbf{D}$ is drillers logs to be used to calibrate stratigraphy model parameters.

Principal Findings and Significance

(1) Stratigraphy model calibration

For results and discussion, we use the following short forms. The first level of uncertainty has three propositions, which are Exponential (Exp), Gaussian (Gus) and Pentspherical (Pen) variogram models. The second level has global (G) and local (L) stationarity assumptions. The third level has the calibration data set with an interpretation favoring more sand (D1) or more clay (D2). The fourth level of uncertain has the geological conceptualization with respect to the Denham Springs-Scotlandville Fault resulting into two zones (Z2) or three zones (Z3) model. For example, Z3D1LExp is the name of a model with three subdomains (Z3), using the first calibration data set (D1), local stationarity assumption (L) and Exponential variogram model

(Exp).

To account for all the modeling propositions, we calibrated 24 models for the IK sand-clay cut-off ratio and the dipping angle for horizontal correlation. The best model is Z3D1LExp. The minimum, mean and maximum cut-off ratios of the 24 models are 0.3879, 0.4092 and 0.4389 respectively. These ratios are in agreement with the 0.402±0.0013 mean estimated sand ratio of the 24 models, and the calculated sand ratios from the driller logs data set 1, driller logs data set 2 and resistively logs being 0.3731, 0.4041 and 0.395 respectively. Unlike previous IK studies [Johnson and Dreiss, 1989; Falivene, 2007], which consider at cut-off ratio of 0.5 as a reasonable assumption, this study shows that cut-off ratio can be viewed as probabilities of occurrence as suggested by Chiles and Delfiner [1999], and that a fixed cut-off 0.5 may result in over and under estimation. The calibration results of the 24 models show minimum, mean and maximum dipping angle percentages to be 0.30, 0.56 and 0.79 respectively. This agrees with the geological assumption that the aquifer system is dipping southward [Griffith 2003]. The mean dipping angle and range are in good agreement with the 0.52% dipping angle as estimated from the geophysical logs of boreholes BR-1268 and BR-1028 in the BB' cross section in Griffith [2003].

Figure 2 shows the stratigraphy of the "1,200-foot", "1,500-foot", "1,700-foot" and "2,000-foot" sands between the Denham Springs-Scotlandville Fault and the Baton Rouge Fault for the best model, Z3D1LExp. To verify the correctness of the stratigraphy, we plot municipal and industrial pumping wells and USGS observation wells into the figure and confirm that all the screen intervals are in the sand portion. Figure 2 demonstrates the first time ever that we are able to understand the Baton Rouge aquifer system in detail. From Figure 2, the "1,200-foot", "1,500-foot", and "1,700-foot" interconnect in the area close to the Baton Rouge Fault. Figure 2 also shows four sands between the "1,200-foot" sand and "2,000-foot" sand. There is a distinct clay bed separates the "2,000-foot" sand from its overlying sand. Figure 2 also allows us to verify USGS well naming, facilitate determination of new monitoring wells, and locate proper depth for remediation designs.

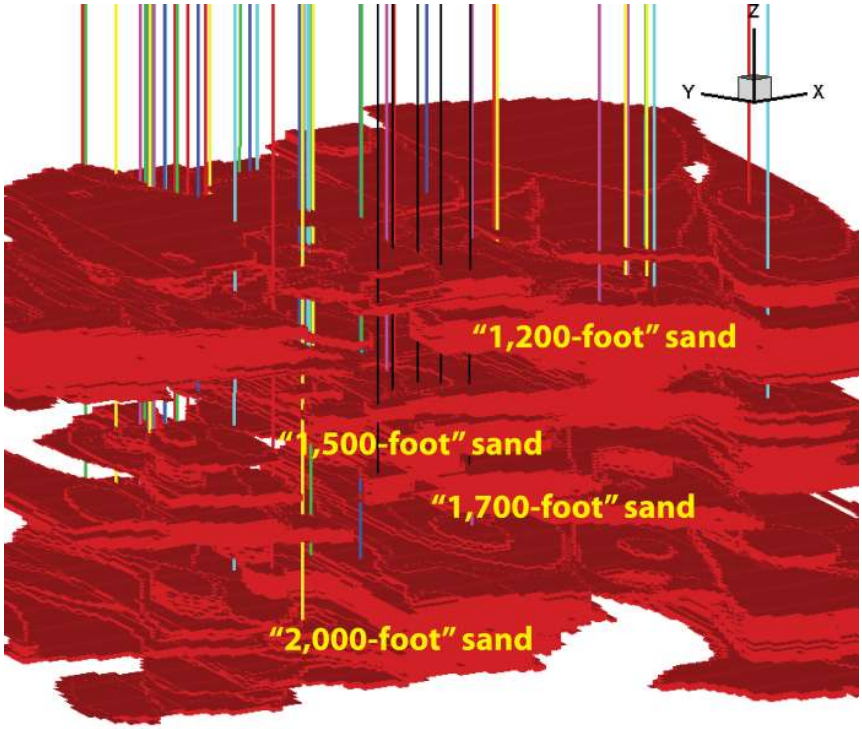

Figure 2: Stratigraphy of the "1,200-foot", "1,500-foot", "1,700-foot" and "2,000-foot" sands between the Denham Springs-Scotlandville Fault and the Baton Rouge Fault. The vertical lines are pumping wells and USGS observation wells.

Using the best model, Figure 3 shows the stratigraphy of the Baton Rouge Fault (BR Fault) and the Denham Springs-Scotlandville Fault (DSS Fault) for the northern face and the southern face. Juxtaposition of the two faces immediately locates the possible leaky areas for the Baton Rouge Fault to allow saltwater to encroach into the freshwater aquifers. Due to large downthrow, sand connection through the Baton Rouge Fault is limited. However, it is clear to see that there is an enormous area that the "1,500-foot" sand north of the Baton Rouge Fault connects the "1,200-foot" sand south of the fault. The leaky area of the Baton Rouge Fault for the "2,000-foot" sand is very small. This may explain why saltwater intrusion in the "1,500-foot" sand is much severer than in the "2,000-foot" sand. The Denham Springs-Scotlandville Fault shows better hydraulic connection through the fault.

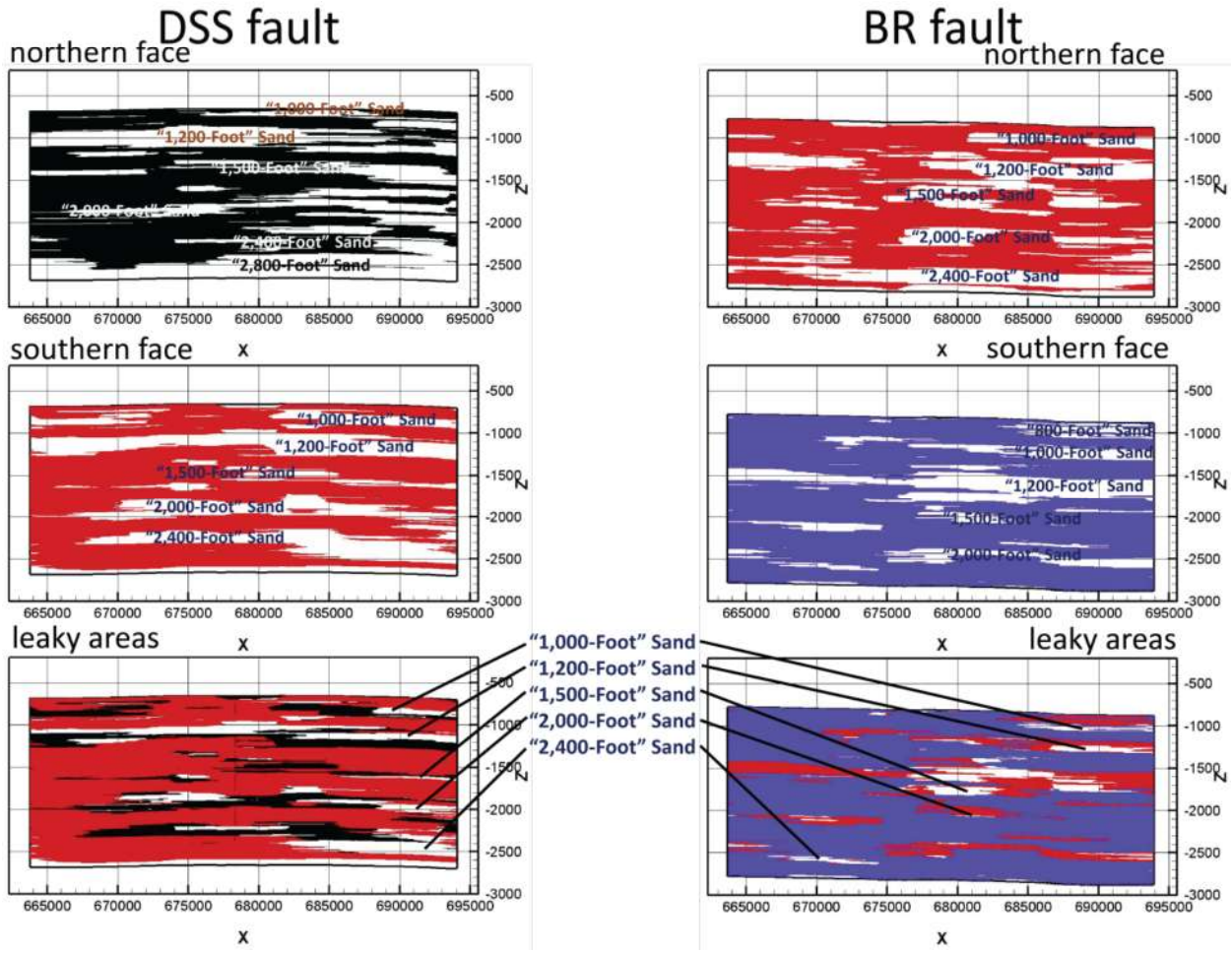

Figure 3: Stratigraphy of the Baton Rouge Fault and the Denham Springs-Scotlandville Faults. Blank areas are sands. The leaky areas through the faults are identified by juxtaposing the northern face and the southern face of the fault stratigraphy.

(2) Model weights

We calculate the model weights using both Occam's widow and different variance windows. The best model has the BIC_{min} being 3.707×10^4. The numbers of data points are 31500. Due to the large data size, the Occam's window as expected singles out only the best model. Tsai and Li [2008b] provide a table for the scaling factors for 1% and 5% significance levels for three σ_D,

which are used here. Model weights of less influential models increase as the significance levels and number of sigma increase that consecutively decrease the weights of the significant the models. Model Z3D1LExp shows to be the only significant model since it only decreased in weight, while all other models increased under all the variance windows.

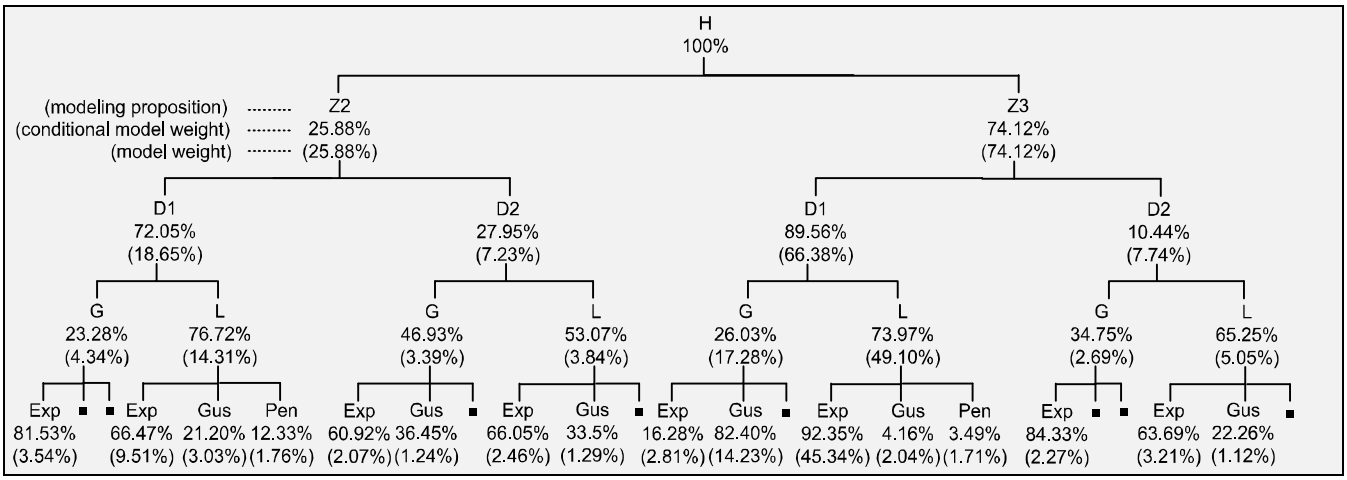

Figure 4. The BMA tree of model weights and conditional model weights for 24 models. Dots present models with model weight less than 1%.

The BMA tree of model weights and conditional model weights for 24 models is shown in Figure 4. The best model is Z3D1LExp, which has a model weight of 45.34%. Exponential models generally tend to perform better than the Gaussian and Pentspherical models, which tend to show similar results. Other modeling propositions of model Z3D1LExp, which are local stationarity (L), first data set (D1) and three subdomains (Z3), tend perform better than other competing propositions. As expected, the worst model is Z2D2GPen, which does not share a single proposition with the best model. The second worst model Z2D2LPen shares only local stationarity (L) proposition with the best model.

(3) Uncertain propagation

Smaller variance windows can be used when one is certain that only the best model is the significant model. Large variance windows are used when this is not intuitively clear and to avoid underestimating the variance. For our purpose, we use large variance window of 5% with 3σ to increase the variance estimation to clearly understand the variance propagation of the within model variance (WMV), between model variance (BMV) and total model variance (TMV). The total uncertainty at each level as expressed by the TMV is the summation of the BMV and WMV at this level. For this purpose, we present a 2D cross section of the south side of the DSS fault with a grid spacing of 50 m in the horizontal direction and 1 foot (0.304 m) in the vertical direction. The X-axis of all the plots is in [m] to agree with UTM-NAD83 coordinate system and the Y-axis is in [foot] to agree with the aquifer nomenclature in the study region.

To better understand the uncertainly propagation, we discuss the WMV, BMW and TMV for the branch of the best model starting with Z3D1L model at level one followed by Z3D1 model at level two , Z3 model at level three and HBMA model at level four. The four plots in Figure 5 show the BMV for the four uncertainty levels, which illustrates the previous remark that the BMV at a certain level is independent from the BMV at other levels. Another remarkable

observation is that the Z3D1L Z3D1 and Z3 BMA models have similar uncertainly patterns, yet with different values. The similar uncertainly patterns indicate again that the best model is dominating the BMV. Different values indicate the importance of different propositions at different level. This means that local and global variogram models are both good propositions as indicated by the high BMV values of Z3D1. On the other hand, the low BMV of Z3 indicates that the using different calibration data sets, which results in different dipping angle and cut-off values, has small impact on uncertainty. By comparing Z3D1L, Z3D1 and Z3 models with the HBMA model, we observe different pattern of uncertainty. This shows that the two subdomains and three subdomains propositions produces relatively different estimations, which is depicted in Figure 5.

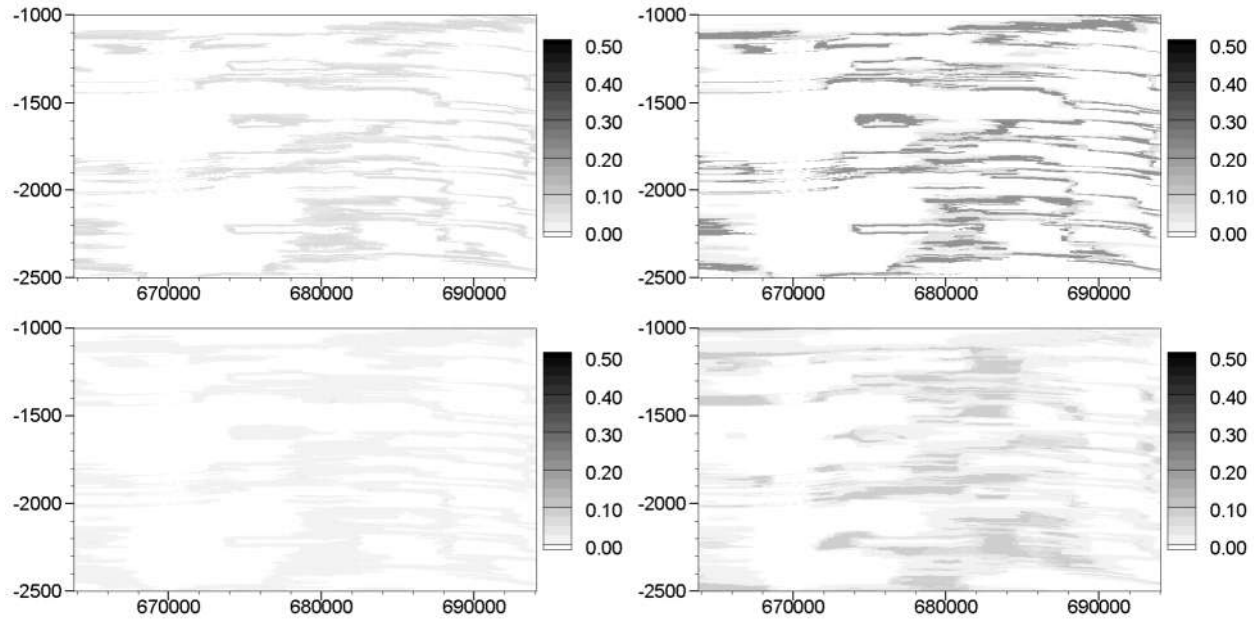

Figure 5. BMV at south side of DSS fault for BMA models Z3D1L, Z3D1, Z3 and HBMA

The WMV at the first level averages the IK variance of all sub-models in each branch, and averages the TMV of the BMA models at higher levels. The Z3D1L BMA model in Figure 6 shows the averaging of the IK variance of the three calibrated models Z3D1LExp, Z3D1LGus and Z3D1LPen. Regions with close proximity to the geophysical logs have lower variance values. This is expected since Kriging variance depends only on the distance from the observation points in which the variance of the estimation error is zero at the data location, and regions with less data have higher variance. The vertical strips of high uncertainty values of the Z3D1 model in Figure 6 illustrates that the WMV in the second level is based on the TMV of the first level. In addition, the WMV sub-plots of Z3 model and HBMA model in Figure 6, illustrate the previous remake that the WMV does not monotonically increase in value, yet more uncertainly regions are being added. This provides an important remark that the regions of uncertainty will always increase by adding more sources of uncertainty, but the variance values can decrease.

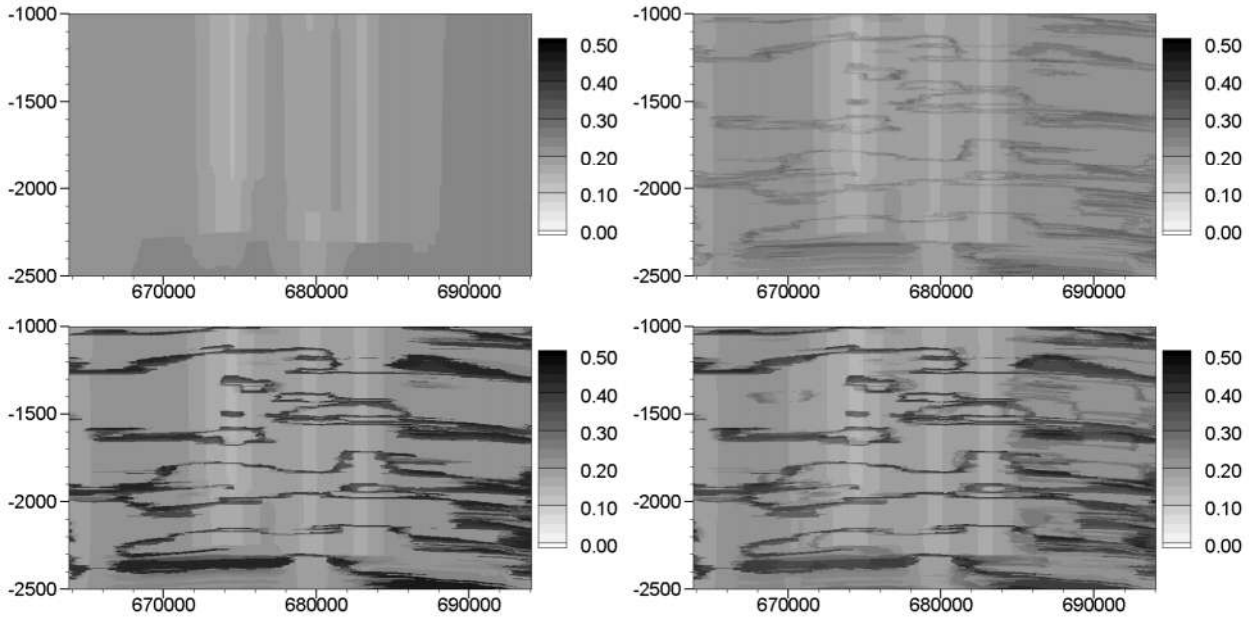

Figure 6. WMV at south side of DSS fault for BMA models Z3D1L, Z3D1, Z3 and HBMA.

The last part of the variance discussion is the TMV, which represents the total uncertainty. The first sub-plot of Figure 7 shows the TMV adds the BMV and WMV. The propagation of uncertainty and the monotonic adding up of uncertainty for the branch of the best model is clearly depicted in Figure 7. Another noticeable remake is that the BMV is taking over the WMV, which indicates that uncertainty due to different levels of uncertainty and competing propositions in each level is higher than the uncertainty arising from the different IK variances of the competing models.

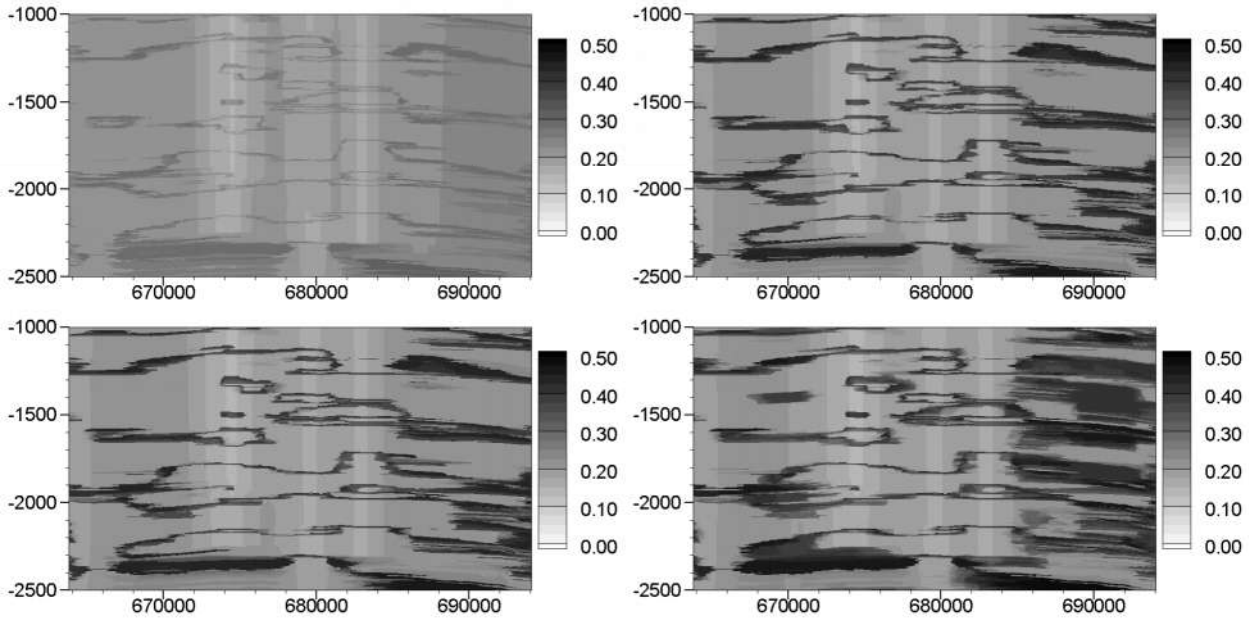

Figure 7. TMV at south side of DSS fault for BMA models Z3D1L, Z3D1, Z3 and HBMA.